JACC: CARDIOVASCULAR IMAGING VOL. 7, NO. 8, 2014

ISSN 1936-878X/$36.00
PUBLISHED BY ELSEVIER INC. http://dx.doi.org/10.1016/j.jcmg.2014.03.013

CMR–Based Identification of Critical Isthmus Sites of Ischemic and Nonischemic Ventricular Tachycardia

Sebastiaan R.D. Piers, MD,* Qian Tao, PhD,† Marta de Riva Silva, MD,* Hans-Marc Siebelink, MD, PhD,* Martin J. Schalij, MD, PhD,* Rob J. van der Geest, PhD,† Katja Zeppenfeld, MD, PhD*

ABSTRACT

OBJECTIVES This study evaluates whether contrast-enhanced (CE) cardiac magnetic resonance (CMR) can be used to identify critical isthmus sites for ventricular tachycardia (VT) in ischemic and nonischemic heart disease.

BACKGROUND Fibrosis interspersed with viable myocytes may cause re-entrant VT. CE-CMR has the ability to accurately delineate fibrosis.

METHODS Patients who underwent VT ablation with CE-CMR integration were included. After the procedure, critical isthmus sites (defined as sites with a ≥11 of 12 pacemap, concealed entrainment, or VT termination during ablation) were projected on CMR-derived 3-dimensional (3D) scar reconstructions. The scar transmurality and signal intensity at all critical isthmus, central isthmus, and exit sites were compared to the average of the entire scar. The distance to >75% transmural scar and to the core-border zone (BZ) transition was calculated. The area within 5 mm of both >75% transmural scar and the core-BZ transition was calculated.

RESULTS In 44 patients (23 ischemic and 21 nonischemic, left ventricular ejection fraction 44 ± 12%), a total of 110 VTs were induced (cycle length 290 ± 67 ms). Critical isthmus sites were identified for 78 VTs (71%) based on ≥11 of 12 pacemaps (67 VTs), concealed entrainment (10 VTs), and/or termination (30 VTs). The critical isthmus sites, and in particular central isthmus sites, had high scar transmurality and signal intensity compared with the average of the entire scar. Of the pacemap, concealed entrainment, and termination sites, 74%, 100%, and 84% were within 5 mm of >75% transmural scar, and 67%, 100%, and 94% were within 5 mm of the core-BZ transition, respectively. The areas within 5 mm of both >75% transmural scar and the core-BZ transition (median 13% of LV) contained all concealed entrainment sites and 77% of termination sites.

CONCLUSIONS Both in ischemic and nonischemic VT, critical isthmus sites are typically located in close proximity to the CMR-derived core-BZ transition and to >75% transmural scar. These findings suggest that CMR-derived scar characteristics may guide to critical isthmus sites during VT ablation. (J Am Coll Cardiol Img 2014;7:774–84) © 2014 by the American College of Cardiology Foundation.

The aim of ventricular tachycardia (VT) ablation is to eliminate critical isthmuses, which can be identified by pacemapping, entrainment mapping, and termination of VT by ablation. The application of these techniques is limited by the inducibility of multiple and often hemodynamically-untolerated VTs, the intramural location of some critical isthmuses, epicardial fat, and other factors.

Fibrotic areas interspersed with viable myocytes can form the substrate for re-entrant VTs. Contrast-enhanced (CE) cardiac magnetic resonance (CMR) can accurately delineate areas with dense

From the *Department of Cardiology, Leiden University Medical Centre, Leiden, the Netherlands; and the †Department of Radiology, Division of Image Processing, Leiden University Medical Centre, Leiden, the Netherlands. The Department of Cardiology, Leiden University Medical Centre, receives unrestricted research grants from Boston Scientific, Medtronic, and Biotronik. Dr. van der Geest has served as a consultant for Medis Medical Imaging Systems. Dr. Zeppenfeld receives consulting fees from St. Jude Medical. All other authors have reported that they have no relationships relevant to the contents of this paper to disclose.

Manuscript received February 24, 2014; revised manuscript received March 13, 2014, accepted March 19, 2014.

fibrosis, and CE-CMR–derived data have been successfully integrated with electroanatomical maps (EAMs) during VT ablation with high registration accuracy (1–7). Integrated CE-CMR scar data may guide to the scar area and uncover intramural and subepicardial scars (1–4).

SEE PAGE 785

Although CE-CMR may help to identify scar areas causing VT, there are limited data on specific CMR-derived scar characteristics at critical isthmus sites, which may be useful to guide ablation. Features of interest are scar transmurality, which has been associated with slow conduction (2,4,7,8), and signal intensity (SI), which has been used to identify conducting channels (5,6) and to delineate core scar and border zone (BZ). Importantly, to date, no study has analyzed the value of CMR-derived scar characteristics to identify areas containing critical isthmuses, thereby potentially guiding substrate-based VT ablation.

The aims of the present study are: 1) to assess CMR-derived scar characteristics at critical isthmus sites of ischemic and nonischemic VT; and 2) to determine the potential value of CMR to delineate areas containing critical isthmus sites for imaging-guided VT ablation.

METHODS

PATIENTS. The study population consisted of 44 of 48 consecutive patients with prior myocardial infarction (MI) (n = 23) or nonischemic cardiomyopathy (NICM) (n = 21) who underwent VT ablation with integration of CE-CMR. Three patients were excluded because of noninterpretable CE-CMR, and 1 was excluded because critical isthmus sites could not be reliably identified due to noninducibility of VT.

The diagnosis of prior MI was based on the presence of significant coronary artery disease (≥70% stenosis on coronary angiography) and subendocardial or transmural late gadolinium enhancement (LGE) in a coronary artery perfusion territory. The diagnosis of NICM was based on the exclusion of significant coronary artery disease, congenital heart disease, hypertrophic cardiomyopathy, arrhythmogenic right ventricular cardiomyopathy, left ventricular (LV) noncompaction, restrictive cardiomyopathy, (sub) acute myocarditis, cardiac sarcoidosis, tachycardia-induced cardiomyopathy, and primary valvular abnormalities. All patients were treated according to our standard clinical protocol and provided informed consent.

CE-CMR ACQUISITION AND PROCESSING. CE-CMR was performed on a 1.5-T Gyroscan ACS-NT/Intera MR system or on a 3.0-T Ingenia MR system (Philips Medical Systems, Best, the Netherlands). A standardized protocol was followed, including cine CMR in long (2- and 4-chamber views) and short axis. In addition, the proximal aorta was imaged using a black-blood turbo spin-echo sequence. Contrast-enhanced images were acquired 15 min after bolus injection of gadolinium (Magnevist, Schering, Berlin, Germany) (0.15 mmol/kg) with an inversion-recovery 3D turbo-field echo sequence with parallel imaging. The heart was imaged in 1 or 2 breath-holds with 20 to 24 imaging levels in short-axis views.

Using MASS software (research version 2012, LKEB, Leiden University Medical Centre, Leiden, the Netherlands), the centerline of the proximal coronary arteries and the luminal boundary of the proximal aorta were manually defined in the black-blood spin-echo images. The endocardial and epicardial contours were semiautomatically detected on the short-axis images. The defined geometries of the proximal coronary arteries, aorta, and myocardial boundaries were converted into 3D meshes. Scar was defined as myocardium with SI ≥35% of maximal myocardial SI, and was subdivided into core scar (>50% of maximal SI) and BZ (35% to 50% of maximal SI) according to the method described by Roes et al. (9). The vertices of the LV endocardial and epicardial meshes were color-coded for scar transmurality for the inner and outer one-half of the wall, respectively. All meshes were imported into the CARTO system using CartoMerge image integration software (Biosense Webster Inc., Diamond Bar, California). On the CARTO 3 system, scars were also visualized as 3D structures, which were created using MATLAB software version 2012a (MathWorks Inc., Natick, Massachusetts).

ELECTROPHYSIOLOGICAL EVALUATION. Antiarrhythmic drugs were discontinued for ≥5 half-lives with the exception of amiodarone. Programmed electrical stimulation consisted of 3 drive cycle lengths (600, 500, and 400 ms) with 1 to 3 ventricular extrastimuli (≥200 ms) from ≥2 right ventricular sites and burst pacing (cycle length ≥200 ms), which was repeated with isoprenaline (2 to 10 μg/min) when necessary. The positive endpoint for stimulation was induction of a monomorphic VT lasting for >30 s or requiring termination because of hemodynamic compromise.

ELECTROANATOMICAL MAPPING, REAL-TIME IMAGE INTEGRATION, AND ABLATION. If indicated, epicardial access was first obtained through subxiphoid puncture. Then, heparin was administered

ABBREVIATIONS AND ACRONYMS

BZ = border zone
CE = contrast enhanced
CMR = cardiac magnetic resonance
EAM = electroanatomical mapping
IQR = interquartile range
LGE = late gadolinium enhancement
LV = left ventricle
MI = myocardial infarction
NICM = nonischemic cardiomyopathy
SI = signal intensity
VT = ventricular tachycardia

and EAM was performed using a 3.5-mm irrigated-tip catheter (NaviStar ThermoCool, Biosense Webster Inc.) and the CARTO system. Limited EAM of the aortic root was performed, and the position of the left main coronary artery, confirmed by contrast injection through the mapping catheter, was tagged on the map. CE-CMR-derived images were visually aligned with the EAM using the left main landmark. Then, the LV was mapped retrogradely focusing on the integrated CMR-derived scar. The LV surfaces of CMR and EAM were aligned with the translation tool provided by the mapping system until the lowest mean surface registration error was reached. Multidetector computed tomography-derived coronary artery anatomy and epicardial fat meshes were integrated with the EAM in patients undergoing epicardial mapping (4,10).

Potential ablation target sites were identified by activation mapping and entrainment mapping for stable VT. For unstable VT, the area of interest was identified by substrate mapping and detailed pacemapping. To confirm the best pacemap site, pacing was repeated after moving the catheter in all possible directions. With the catheter placed in the area of interest, VT was reinduced and briefly mapped to identify diastolic activity and terminate the VT by ablation, also used in cases of hemodynamically-unstable VT.

At the epicardium, ablation was usually withheld when the estimated distance to a coronary artery was <5 mm, as assessed by integrated multidetector computed tomography-derived coronary anatomy and coronary angiography (10). High-output pacing (10 mA, 2 ms) was performed to localize the phrenic nerve. Radiofrequency energy was applied at 30 to 45W (maximum temperature 45°C, flow 20 to 30 ml/min, 60 s) for endocardial sites and ≤50W (flow 20 ml/min) for epicardial sites.

ACUTE AND LONG-TERM OUTCOME. After ablation, the entire programmed electrical stimulation protocol was repeated. Isoprenaline was administered if required to induce VT before ablation. Complete procedural success was defined as noninducibility of any sustained monomorphic VT; partial success as elimination of the (presumed) clinical VT but persistent inducibility of ≥1 nonclinical VT; and failure as persistent inducibility of the (presumed) clinical VT. Patients were followed up at 3, 6, and 12 months after ablation and at 6- to 12-month intervals thereafter.

CRITICAL ISTHMUS SITES. For the current analysis, all studies were thoroughly reviewed on the electrophysiology recording system (Prucka Cardiolab recording system, Houston, Texas) with an observer who was blinded to the electroanatomical maps. Critical isthmus sites were defined by the following criteria:

1. ≥11 of 12 pacemaps (precise match of major deflections *and* all subtle notches in ≥11 of 12 leads; site with longest S-QRS delay in case of identical match);

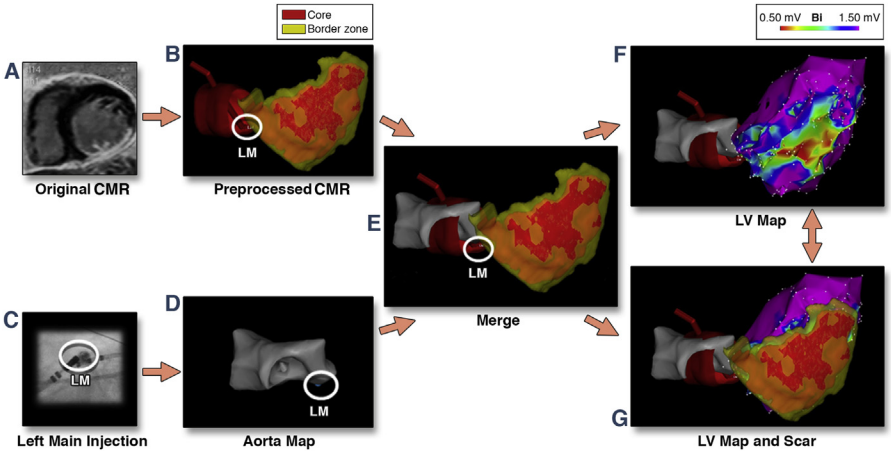

FIGURE 1 Integration of CMR-Derived 3D Scar Reconstruction With Electroanatomical Maps

Before the procedure, the original cardiac magnetic resonance (CMR) **(A)** is processed to create a three-dimensional (3D) scar reconstruction **(B)**. During the procedure, the position of the left main (LM) is confirmed by contrast injection **(C)** and tagged on the map **(D)**. The CMR data are subsequently integrated with the electroanatomic map based on the LM landmark **(E)**. Left ventricular (LV) mapping can then be focused on the CMR-derived scar **(F and G)**.

2. Concealed entrainment with post-pacing interval equal to tachycardia cycle length; and/or
3. VT slowing and termination during ablation.

Critical isthmus sites for the same VT could be identified by >1 criterion. Because of differences in accuracy between pacemapping, entrainment, and termination, we have stratified the analysis for these different criteria. Critical isthmus sites were further subdivided into central isthmus sites (S-QRS or E-QRS 31% to 70% of VT cycle length) and exit sites (S-QRS or E-QRS 0% to 30% of VT cycle length).

The LV endocardial low bipolar (≤1.50 mV) and unipolar (≤8.27 mV [11]) voltage areas were measured in all patients, and the epicardial low bipolar (≤1.81 mV [4]) and unipolar (≤7.95 mV [4]) voltage areas were measured in patients with NICM who underwent epicardial mapping. The location of LV endocardial critical isthmus sites with respect to the endocardial low voltage areas was assessed in all patients. The location of LV epicardial critical isthmus sites with respect to epicardial areas with low voltage and abnormal electrograms (4) was assessed in patients with NICM.

CONTRAST-ENHANCED CMR-DERIVED 3D SCAR RECONSTRUCTIONS. CMR-derived 3D scar reconstructions and all CMR-based scar parameters were computed using MATLAB software. Examples of scars are displayed in Figures 1 and 2. After the procedure, all mapping points at critical isthmus sites were projected onto the CMR-derived 3D scar reconstructions using MATLAB software (example in Fig. 2). Scar transmurality was calculated by dividing scar thickness by wall thickness. The local scar transmurality and SI at a mapping point were calculated as the mean value within a 5-mm-radius transmural cylinder around the mapping point. The local scar transmurality and SI at critical isthmus sites were compared with the average scar

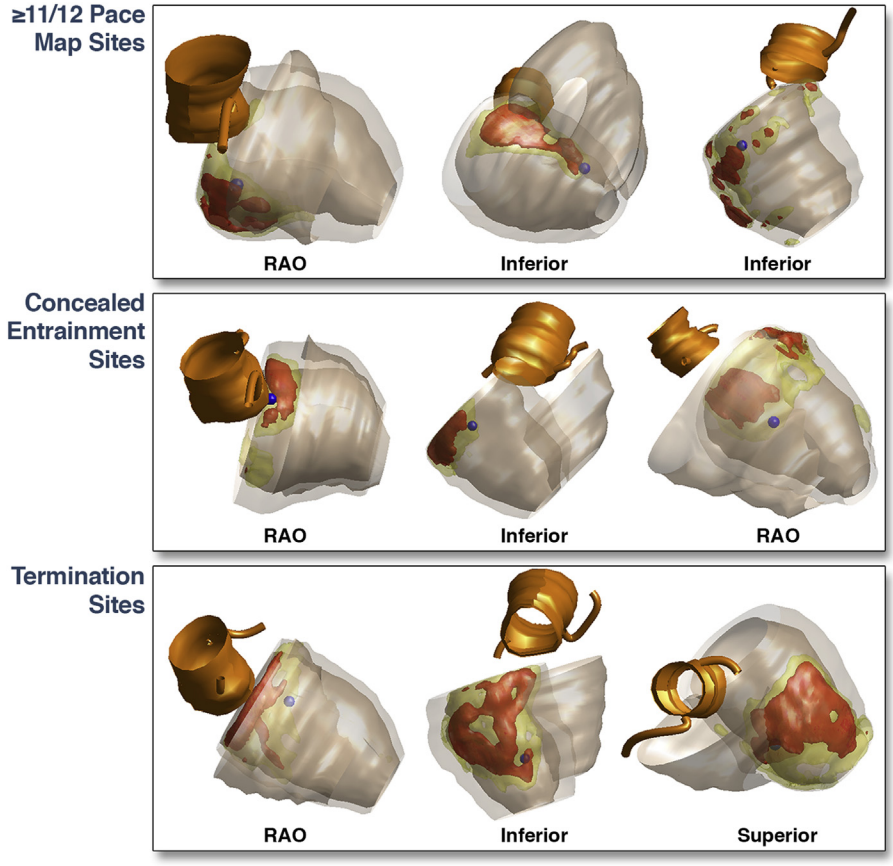

FIGURE 2 Examples of Critical Isthmus Sites Projected on CMR-Derived 3D Scar Reconstructions

RAO = right anterior oblique; other abbreviations as in Figure 1.

transmurality and SI in the same patient. The distances from critical isthmus sites to >75% transmural scar and core-BZ transition were calculated. The core-BZ transition was defined as the line where core and BZ meet, projected on the endocardial or epicardial surface.

TABLE 1 Baseline, Procedural and CMR-Derived Data

	All Patients (n = 44)	Post-Infarction (n = 23)	NICM (n = 21)
Age	62 ± 13	67 ± 9	56 ± 14
Male	37 (84)	20 (87)	17 (81)
NYHA functional class			
I	24 (55)	12 (52)	12 (57)
II	17 (39)	10 (44)	7 (33)
III	3 (7)	1 (4)	2 (10)
LV ejection fraction, %	44 ± 12	45 ± 12	42 ± 11
LV end-diastolic volume, ml	209 (181–253)	203 (174–233)	213 (189–257)
LV end-systolic volume, ml	109 (87–155)	102 (84–134)	124 (89–160)
History of atrial flutter/fibrillation	8 (18)	5 (22)	3 (14)
BMI, kg/m^2	27 ± 5	28 ± 5	27 ± 4
Diabetes mellitus	7 (16)	5 (22)	2 (10)
eGFR <60 ml/min	5 (11)	3 (13)	2 (10)
Number of VTs induced			
1	17 (39)	12 (52)	5 (24)
2	13 (30)	4 (17)	9 (43)
≥3	14 (31)	7 (31)	7 (33)
Hemodynamic stability of VTs			
Only stable VT	12 (27)	7 (30)	5 (24)
Only unstable VT	18 (41)	8 (35)	10 (48)
Stable and unstable VT	14 (32)	8 (35)	6 (29)
Mean cycle length of induced VTs, ms	292 ± 65	292 ± 63	292 ± 68
Pericardial puncture	15 (34)	2 (9)	13 (62)
Radiofrequency energy applications			
Only endocardial	31 (71)	21 (91)	10 (48)
Only epicardial	4 (9)	1 (4)	3 (14)
Endocardial and epicardial	8 (18)	1 (4)	7 (33)
None	1 (2)	0 (0)	1 (5)
Procedural outcome			
Complete success	26 (59)	15 (65)	11 (52)
Partial success	9 (21)	3 (13)	6 (29)
Failure	5 (11)	1 (4)	4 (19)
Indeterminate	4 (9)	4 (17)	0 (0)
Procedural duration, min	201 ± 73	179 ± 51	225 ± 87
Fluoroscopy time, min	44 ± 21	37 ± 16	51 ± 23
CMR scar volume, % of LV wall			
Total scar volume	16 (12–22)	18 (12–23)	15 (11–20)
Core scar volume	6 (4–9)	7 (4–10)	6 (4–8)
BZ volume	10 (7–12)	10 (8–12)	9 (7–13)
CMR scar area, % of endocardial LV			
Area of ≤50% transmural scar	15 (12–19)	13 (11–16)	17 (13–24)
Area of 51%–75% transmural scar	7 (4–10)	9 (5–12)	6 (4–9)
Area of >75% transmural scar	6 (3–10)	7 (3–13)	4 (2–7)

Values are mean ± SD, n (%), or median (interquartile range).

BMI = body mass index; BZ = border zone; CMR = cardiac magnetic resonance; eGFR = estimated glomerular filtration rate; LV = left ventricular; NICM = nonischemic cardiomyopathy; NYHA = New York Heart Association; VT = ventricular tachycardia.

The following pre-defined areas were calculated for the endocardium and epicardium in each patient: CMR-derived scar, area within 5 mm of >75% transmural scar, area within 5 mm of core-BZ transition, and areas within 5 and 10 mm of the core-BZ transition with >75% scar transmurality. The percentage of critical isthmus sites located within these areas was calculated.

CMR-derived overall scar characteristics were calculated, including total scar volume, core volume, BZ volume, and areas of ≤50%, 51% to 75%, and >75% transmural scar. The relation was assessed between these characteristics and: 1) average cycle length of induced VTs; 2) number of induced VTs; 3) inducibility of VT after ablation; and 4) VT recurrence.

STATISTICAL ANALYSIS. Categorical variables are displayed as number (percentage) and continuous variables are expressed as mean ± SD or median (interquartile range [IQR]). Continuous variables were compared using the Student *t* test when normally distributed or the Mann-Whitney *U* test when non-normally distributed. For paired variables, the paired *t* test or the Wilcoxon signed rank test were used, respectively. The relation between CMR-derived overall scar characteristics and the number of induced VTs and average cycle length of induced VTs was first analyzed by univariate linear regression analysis. The relation with VT inducibility after ablation was analyzed by univariate logistic regression and the relation with VT recurrence by univariate Cox regression. When statistically significant associations were identified in univariate analyses, multivariate analyses were performed to assess the independent associations between the scar characteristics of interest and the VT or outcome parameters. All analyses were performed with SPSS version 20.0 (IBM, Somers, New York). All tests are 2-sided, and p values <0.05 were considered significant.

RESULTS

A total of 44 patients (23 post-MI and 21 NICM, age 62 ± 13 years, CMR-based left ventricular ejection fraction 44 ± 12%) underwent VT ablation with integration of CMR-derived scar (178 ± 76 LV mapping points; average registration error 3.8 ± 0.6 mm, example in Fig. 1). Epicardial mapping was performed in 15 patients (13 NICM, 2 post-MI; 174 ± 99 mapping points). Baseline and procedural data are provided in Table 1. A total of 110 distinct VTs (cycle length 290 ± 67 ms) could be induced during the procedure. A ≥11 of 12 pacemap was obtained in 67 VTs (61%; median S-QRS 30 ms [IQR: 10 to 48 ms]). Entrainment was concealed with post-pacing interval

equaling VT cycle length in 10 VTs (9%; median E-QRS 98 ms [IQR: 61 to 133 ms]). Thirty-one VTs (28%) slowed and terminated during ablation (median E-QRS before ablation 96 ms [IQR: 37 to 126 ms]; median time to termination 9 s, [IQR: 6 to 11 s]). Based on these findings, critical isthmus sites could be identified in 78 of 110 VTs (71%) at the following locations: LV endocardium (46 VTs, 59%), epicardium (16 VTs, 21%), right ventricular septum (7 VTs, 9%), aortic root (5 VTs, 6%), both aortic root and LV endocardium (2 VTs, 3%), both right ventricular endocardium and epicardium (1 VT, 1%) and anterior cardiac vein (1 VT, 1%). Complete procedural success was achieved in 26 patients (59%), partial success in 9 (21%), failure in 5 (11%), and the acute outcome was indeterminate in 4 (9%) due to noninducible clinical VT prior to ablation.

SCAR TRANSMURALITY, SIGNAL INTENSITY, AND DISTANCE TO CORE-BZ TRANSITION AT CRITICAL ISTHMUS SITES. The mapping points at critical isthmus sites were successfully projected on the CE-CMR-derived 3D scar reconstructions (examples in Fig. 2). One epicardial VT originated from the right ventricular outflow tract and was excluded from further analyses. Sites with a ≥11 of 12 pacemap had a scar transmurality of 66 ± 22% compared with an average scar transmurality in the same patients of 59 ± 12% (p = 0.005) (Fig. 3). The difference in transmurality was larger at concealed entrainment sites (concealed entrainment 76 ± 16% vs. average 62 ± 10%, p = 0.024) and termination sites (termination 70 ± 21% vs. average 62 ± 12%, p = 0.018).

The scar SI at critical isthmus sites was higher than the average scar SI in the same patients (≥11 of 12 pacemap 68 ± 24% vs. average 59 ± 16%, p = 0.001; concealed entrainment 72 ± 21% vs. average 58 ± 15%, p = 0.074; termination 69 ± 21% vs. average 59 ± 15%, p = 0.010) (Fig. 3).

The median distance to >75% transmural scar was 1.5 mm (IQR: 0.0 to 5.6 mm) at ≥11 of 12 pacemaps, 0.0 mm (IQR: 0.0 to 3.0 mm) at concealed entrainment sites, and 1.8 mm (IQR: 0.0 to 3.8 mm) at termination sites (Fig. 4). The critical isthmus sites clustered around the core-BZ transition, with a median distance to the transition of 3.7 mm (IQR: 1.5 to 7.0 mm) at ≥11 of 12 pacemaps, 1.9 mm (IQR: 0.0 to 2.6 mm) at concealed entrainment sites, and 2.5 mm (IQR: 1.1 to 4.2 mm) at termination sites.

SCAR CHARACTERISTICS AT EXIT AND ISTHMUS SITES. Based on pacemapping, exit sites could be identified in 60 VTs and central isthmus sites in 6 VTs. Scar transmurality and SI were higher at pacemapping-based central isthmus and exit sites,

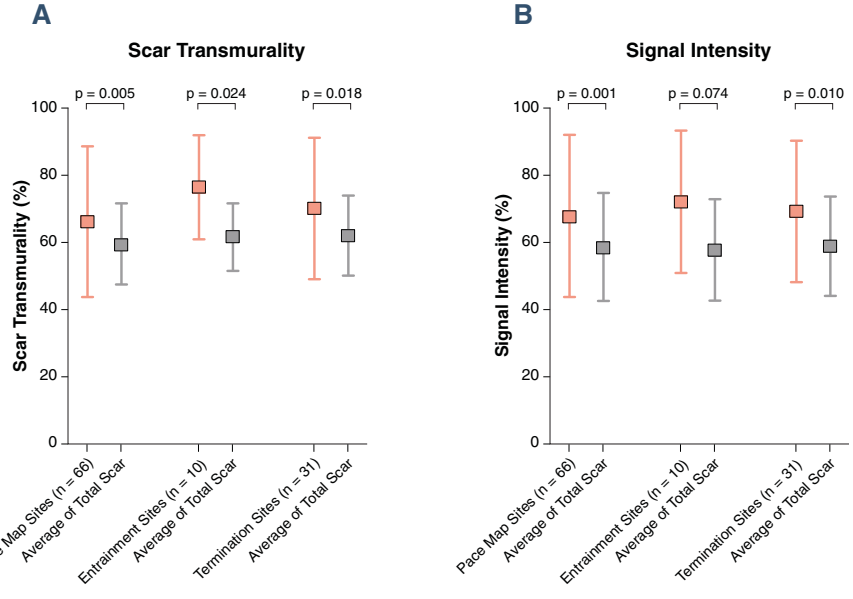

FIGURE 3 Scar Transmurality and SI at Critical Isthmus Sites

Scar transmurality and signal intensity (SI) at critical isthmus sites compared with the average scar transmurality and SI in the same patient. Values are mean ± SD.

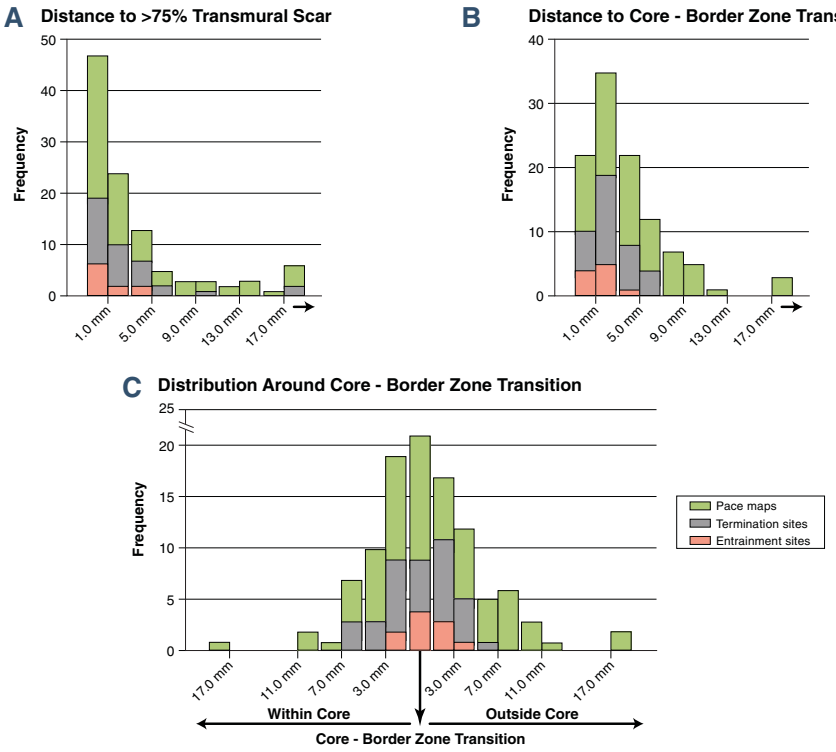

FIGURE 4 **Distance From Critical Isthmus Sites to >75% Transmural Scar and the Core-BZ Transition**

(A) The distance from critical isthmus sites to >75% transmural scar, and **(B)** the distance to the core-border zone (BZ) transition. **(C)** The remarkable bell-shaped distribution of critical isthmus sites around the core-BZ transition.

compared with the average (Fig. 5). The differences were more pronounced at central isthmus sites (transmurality 78 ± 14% vs. average 64 ± 8%, p = 0.051; SI 77 ± 17% vs. average 59 ± 6%, p = 0.012), than at exit sites (transmurality 65 ± 23% vs. average 59 ± 12%, p = 0.019; SI 67 ± 25% vs. average 59 ± 17%, p = 0.004).

Of the 31 termination sites, 16 (52%) were consistent with an exit site and 15 (48%) with a central isthmus site. Scar transmurality was above average at central isthmus sites (75 ± 22% vs. 60 ± 13%, p = 0.008), but not at exit sites (66 ± 19% vs. 63 ± 10%, p = 0.58). Similarly, SI was above average at central isthmus sites (74 ± 21% vs. 56 ± 13%, p = 0.006), but not at exit sites (65 ± 21% vs. 62 ± 15%, p = 0.54). The number of concealed entrainment sites was too small for subgroup analyses.

NONISCHEMIC CARDIOMYOPATHY VERSUS POST-MYOCARDIAL INFARCTION. At ≥11 of 12 pacemaps and termination sites, the CMR-derived scar characteristics (including scar transmurality, SI, distance to >75% transmural scar, and distance to core-BZ transition) were not significantly different between patients with NICM or prior MI (all p > 0.05, data not shown).

CMR-BASED IDENTIFICATION OF CRITICAL ISTHMUS SITES. The CMR-derived scar area (median 24% of LV [IQR: 16% to 30%]) contained 77% of ≥11 of 12 pacemap sites, 90% of concealed entrainment sites, and 90% of termination sites (Fig. 6A). The area within 5 mm of both >75% transmural scar and core-BZ transition (median 13% of LV [IQR: 7% to 19%]) included only 56% of ≥11 of 12 pacemap sites, but still 100% of concealed entrainment sites and 77% of termination sites.

In post-MI patients, the areas within 5 mm of >75% transmural scar, within 5 mm of the core-BZ transition, and the low bipolar voltage areas were limited in size and contained the majority of LV endocardial critical isthmus sites (Fig. 6B).

For patients with NICM the areas within 5 mm of both >75% transmural scar *and* core-BZ transition (median 13% of LV [IQR: 6% to 19%]), and the LV endocardial low unipolar voltage area (median 11% of

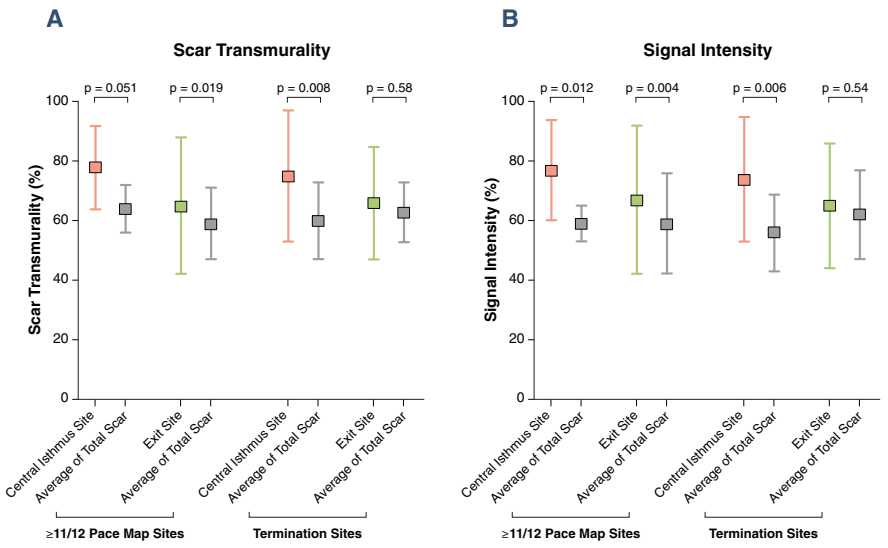

FIGURE 5 Scar Transmurality and SI at Central Isthmus and Exit Sites

Scar transmurality and signal intensity (SI) at central isthmus and exit sites compared with the average scar transmurality and SI in the same patient. Values are mean ± SD.

LV [IQR: 2% to 16%]) were comparably small and contained the majority of LV endocardial critical isthmus sites (Fig. 6C). The LV epicardial low bipolar and unipolar voltage areas with abnormal electrograms were large (median 27% of LV [IQR: 15% to 41%] and median 43% of LV [IQR: 25% to 65%], respectively), whereas the area within 5 mm of both >75% transmural scar *and* the core-BZ transition was smaller (median 12% of LV [IQR: 6% to 19%]) and contained the majority of epicardial entrainment and termination sites (Fig. 6D).

CMR-DERIVED SCAR CHARACTERISTICS, VT CHARACTERISTICS, AND OUTCOME. Univariate analysis revealed that total scar, core and BZ volumes, and areas of 51% to 75% and >75% transmural scar were associated with slower induced VTs (Online Table 1). In a multivariate model including scar transmurality areas, only the area of >75% transmural scar remained associated with VT cycle length (+17 ms per 5 cm^2, 95% confidence interval: 7 to 27 ms, $p = 0.001$). In a multivariate model including the core and BZ volumes, only the BZ volume remained associated with VT cycle length (+20 ms per 5 ml BZ, 95% confidence interval: 9 to 32 ms, $p = 0.001$). BZ volume and area of >75% transmural scar were interrelated ($R^2 = 0.50$, $p < 0.001$) and became nonsignificant if both parameters were included in a model.

None of the overall scar characteristics were associated with the number of induced VTs, inducibility of VT after ablation, or VT recurrence (all $p > 0.20$) (Online Tables 2 to 4).

DISCUSSION

In the present study, critical VT isthmus sites in patients with prior MI or NICM were typically located in close proximity to the CMR-derived core-BZ transition and >75% transmural scar. In particular, central isthmus sites had high scar transmurality and signal intensity compared with the average of the entire scar, suggesting that slow conducting pathways are located within relatively dense and transmural scar. The area within 5 mm of both >75% transmural scar and the core-BZ transition covered a median of 13% of the LV, but contained all concealed entrainment sites and 77% of VT termination sites, allowing CE-CMR-based delineation of relatively small areas containing critical parts of the re-entry circuit. The BZ volume and area of >75% transmural scar were positively correlated with the cycle length of induced VTs, providing further support to the premise that the BZ and >75% transmural scar are associated with slow conduction.

SCAR TRANSMURALITY AND SIGNAL INTENSITY. The current study comprises the largest series of

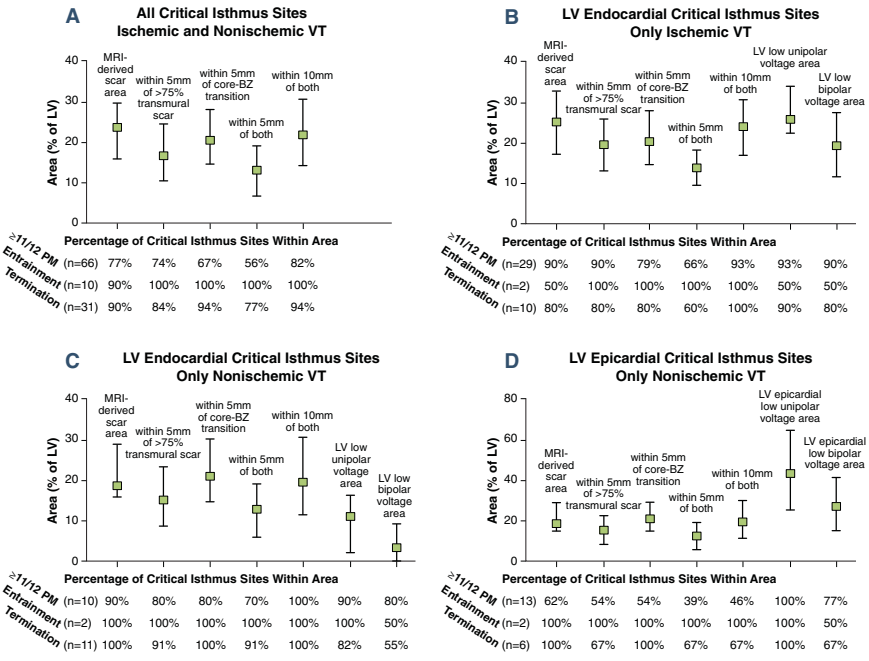

FIGURE 6 Percentage of Critical Isthmus Sites Within Specific Areas

Values are median with interquartile range. BZ = border zone; PM = pacemap; VT = ventricular tachycardia; other abbreviations as in Figure 1.

patients undergoing VT ablation with CE-CMR integration to date, and provides detailed analyses of CMR-derived scar parameters at VT-related sites. Critical isthmus sites were typically located within, or in close proximity to, >75% transmural scar in post-MI and NICM patients. In 1 prior study in 23 post-MI patients, 62% of re-entrant VT critical sites were identified in regions with >75% transmural scar (8). Several studies have demonstrated a strong correlation between electrogram prolongation and scar transmurality (2,4,7,8), which is in line with our finding that the area of >75% transmural scar correlated positively with the cycle length of induced VTs. Scar transmurality may therefore be an important aspect of the substrate for re-entrant VT.

The scar density at critical isthmus sites is reported in only 1 study in 9 patients with ischemic VT, in which 71% of VT isthmus sites were located in the infarct core and 29%were located in the BZ (7). All critical sites in the BZ were in an area of transmural infarct, with SI slightly lower than the cutoff defining core infarct. In the present study, the remarkable bell-shaped distribution of critical isthmus sites around the core-BZ transition suggests that the 50% maximal SI threshold may indicate a critical mix between fibrosis and viable myocytes that allows for slow conduction and, thereby, re-entrant VT.

CMR-derived BZ channels through higher SI scar areas have been correlated with critical isthmus sites (5,6,12). Notably, in the present study we observed relatively high SI at critical isthmus sites, contradicting the premise that VT isthmuses manifest as relatively low SI channels on CE-CMR.

Prior investigations demonstrated differences in scar features between patients with NICM and prior MI. One study demonstrated a lower LGE SI in patients with atypical LGE patterns, compared with patients with an infarct LGE pattern, suggesting that there is a higher scar density in post-MI patients (13). A study in 33 patients with NICM or prior MI who underwent VT ablation showed that patients after MI had more pronounced EAM-based conduction delay than patients with NICM (14). In the current study, we could demonstrate that, although overall scar characteristics may be different, CMR-derived scar characteristics at critical isthmus sites were similar between patients with prior MI or NICM.

CMR-BASED IDENTIFICATION OF THE AREA OF INTEREST. We could demonstrate the added value of CMR-based scar characteristics for identification of areas containing critical isthmus sites during VT ablation. A limited area within 5 mm of both >75% transmural scar and core-BZ transition encompassed all concealed entrainment sites and 77% of termination sites, which are considered to be reliable markers for critical isthmus sites. This area may, therefore, serve as a target area for substrate-guided ablation approaches. Only 56% of ≥11 of 12 pacemap sites was located in these regions. However, ≥11 of 12 pacemaps may also be recorded in the vicinity of exit sites and may therefore be less accurate. Importantly, the CMR-derived target area can be displayed and used as a guide for ablation using single landmark-based image integration without extensive electroanatomical substrate mapping.

STUDY LIMITATIONS. No critical isthmus sites could be identified in 29% of VTs, which may be due to intramural re-entry circuits, epicardial re-entry circuits in patients who did not undergo epicardial mapping, or epicardial re-entry circuits that could not be mapped due to epicardial fat.

Pacemapping is considered to be a less accurate technique for defining critical isthmus sites, in particular if no S-QRS delay is observed. Therefore, we have stratified the analysis for different techniques to identify critical isthmus sites and for different E/S-QRS delays.

Scar transmurality and signal intensity were calculated for a 5mm-radius transmural cylinder, and therefore, they do not depend on the endocardial or epicardial location. The present data can thus not be used to predict whether an endocardial or epicardial ablation procedure will be successful.

Data from endocardial and epicardial critical isthmus sites were pooled, because the distance to >75% transmural scar and core-BZ transition did not differ between endocardial and epicardial pacemapping- or termination-based critical isthmus sites in patients with NICM.

CLINICAL IMPLICATIONS. Based on the present findings, CMR may be used to guide to areas that are likely to contain critical isthmus sites. Within these areas, ablation target sites may be further specified (e.g., based on electrogram characteristics or pacemapping). Importantly, the CMR-derived area of interest is available before extensive substrate mapping and is not limited by intramural or subepicardial location of scars or by epicardial fat. Moreover, it is relatively small compared to low-voltage areas, in particular to epicardial low-voltage areas in NICM. VT cycle length was not different between VTs with and without an identifiable critical isthmus site (294 ± 65 ms vs. 282 ± 70 ms, $p = 0.40$), indicating that both slow and fast VTs are represented in the analysis. CMR may be particularly useful if no or only limited mapping time is available for poorly tolerated fast VT. Future prospective studies are required to assess whether CMR guidance to pre-selected regions that are likely to contain critical isthmus sites may improve the efficiency and efficacy of VT ablation.

CONCLUSIONS

In ischemic and nonischemic VT, critical parts of the re-entry circuit are typically located in close proximity to >75% transmural scar and the core-BZ transition. The area within 5 mm of both >75% transmural scar and core-BZ transition contained all concealed entrainment sites and 77% of termination sites. These findings suggest that CMR-derived scar characteristics may be used to guide to critical isthmus sites during VT ablation.

REPRINT REQUESTS AND CORRESPONDENCE: Dr. Katja Zeppenfeld, Department of Cardiology, Leiden University Medical Center, C-05-P, P.O. Box 9600, 2300 RC Leiden, the Netherlands. E-mail: K.Zeppenfeld@lumc.nl.

REFERENCES

1. Bogun FM, Desjardins B, Good E, et al. Delayed-enhanced magnetic resonance imaging in non-ischemic cardiomyopathy: utility for identifying the ventricular arrhythmia substrate. J Am Coll Cardiol 2009;53:1138–45.

2. Dickfeld T, Tian J, Ahmad G, et al. MRI-guided ventricular tachycardia ablation: integration of late gadolinium-enhanced 3D scar in patients with implantable cardioverter-defibrillators. Circ Arrhythm Electrophysiol 2011;4:172–84.

3. Wijnmaalen AP, van der Geest RJ, van Huls van Taxis CF, et al. Head-to-head comparison of contrast-enhanced magnetic resonance imaging and electroanatomical voltage mapping to assess post-infarct scar characteristics in patients with ventricular tachycardias: real-time image integration and reversed registration. Eur Heart J 2011;32:104–14.

4. Piers SR, van Huls van Taxis CF, Tao Q, et al. Epicardial substrate mapping for ventricular tachycardia ablation in patients with non-ischaemic cardiomyopathy: a new algorithm to differentiate between scar and viable myocardium developed by simultaneous integration of computed tomography and contrast-enhanced magnetic resonance imaging. Eur Heart J 2012;34:586–96.

5. Perez-David E, Arenal A, Rubio-Guivernau JL, et al. Noninvasive identification of ventricular tachycardia-related conducting channels using contrast-enhanced magnetic resonance imaging in patients with chronic myocardial infarction: comparison of signal intensity scar mapping and endocardial voltage mapping. J Am Coll Cardiol 2011;57:184–94.

6. Andreu D, Berruezo A, Ortiz-Perez JT, et al. Integration of 3D electroanatomic maps and magnetic resonance scar characterization into the navigation system to guide ventricular tachycardia ablation. Circ Arrhythm Electrophysiol 2011;4:674–83.

7. Desjardins B, Crawford T, Good E, et al. Infarct architecture and characteristics on delayed enhanced magnetic resonance imaging and electroanatomic mapping in patients with post-infarction ventricular arrhythmia. Heart Rhythm 2009;6:644–51.

8. Sasaki T, Miller CF, Hansford R, et al. Myocardial structural associations with local electrograms: a study of postinfarct ventricular tachycardia pathophysiology and magnetic resonance-based noninvasive mapping. Circ Arrhythm Electrophysiol 2012;5:1081–90.

9. Roes SD, Borleffs CJ, van der Geest RJ, et al. Infarct tissue heterogeneity assessed with contrast-enhanced MRI predicts spontaneous ventricular arrhythmia in patients with ischemic cardiomyopathy and implantable cardioverter-defibrillator. Circ Cardiovasc Imaging 2009;2:183–90.

10. van Huls van Taxis CF, Wijnmaalen AP, Piers SR, van der Geest RJ, Schalij MJ, Zeppenfeld K. Real-time integration of MDCT-derived coronary anatomy and epicardial fat: impact on epicardial electroanatomic mapping and ablation for ventricular arrhythmias. J Am Coll Cardiol Img 2013;6:42–52.

11. Hutchinson MD, Gerstenfeld EP, Desjardins B, et al. Endocardial unipolar voltage mapping to detect epicardial ventricular tachycardia substrate in patients with nonischemic left ventricular cardiomyopathy. Circ Arrhythm Electrophysiol 2011;4:49–55.

12. Fernández-Armenta J, Berruezo A, Andreu D, et al. Three-dimensional architecture of scar and conducting channels based on high resolution ce-CMR: insights for ventricular tachycardia ablation. Circ Arrhythm Electrophysiol 2013;6:528–37.

13. Ugander M, Oki AJ, Hsu LY, et al. Extracellular volume imaging by magnetic resonance imaging provides insights into overt and subclinical myocardial pathology. Eur Heart J 2012;33:1268–78.

14. Nakahara S, Tung R, Ramirez RJ, et al. Characterization of the arrhythmogenic substrate in ischemic and nonischemic cardiomyopathy implications for catheter ablation of hemodynamically unstable ventricular tachycardia. J Am Coll Cardiol 2010;55:2355–65.

KEY WORDS cardiac magnetic resonance, catheter ablation, image integration, myocardial infarction, nonischemic cardiomyopathy, ventricular tachycardia

APPENDIX For supplemental tables, please see the online version of this article.